catalysts

MDPI

Article

Microwave-Assisted Oxidation of N_2 into NO_x over a La-Ce-Mn-O Perovskite Yielding Plasmas in a Quartz Flow Reactor at Atmospheric Pressure

Frederic C. Meunier * and Akim Kaddouri †

Univ Lyon, Université Claude Bernard Lyon 1, CNRS, IRCELYON, 2 Av. Albert Einstein, 69626 Villeurbanne, France
* Correspondence: fcm@ircelyon.univ-lyon1.fr
† Professor Akim Kaddouri has passed away.

Abstract: N_2 oxidation to NO_x is a challenging reaction, and alternative routes to the industrial Ostwald process are of interest. A perovskite under flowing O_2-N_2 mixtures at atmospheric pressure in a quartz tube reactor was irradiated by microwaves (MW), leading to the formation of hot spots and plasmas within the catalyst bed. NO_x concentrations up to 2.5 vol.% in one pass were obtained at 600 W. Using a lower MW power of 100 W led to a pulsed mode yielding lower NO_x concentrations and no noticeable damage to the quartz reactor. The formation of plasma was strongly dependent on the perovskite bed packing. The perovskite acted primarily as a susceptor and likely also as a catalyst, although the proportion of heterogeneous and homogenous reactions could not be determined in the present study. The simple reactor layout allowing operation at atmospheric pressure is promising for the development of practical MW-assisted N_2 fixation technologies.

Keywords: NO_x synthesis; nitrogen fixation; microwave; plasma; NTP

check for updates

Citation: Meunier, F.C.; Kaddouri, A. Microwave-Assisted Oxidation of N_2 into NO_x over a La-Ce-Mn-O Perovskite Yielding Plasmas in a Quartz Flow Reactor at Atmospheric Pressure. *Catalysts* **2024**, *14*, 635. https://doi.org/10.3390/catal14090635

Academic Editor: Yi Cheng

Received: 15 August 2024
Revised: 11 September 2024
Accepted: 17 September 2024
Published: 19 September 2024

1. Introduction

Nitrogen fixation technologies are central to modern chemical industries, but also major contributors to global warming. The industrial production of NO_x, a precursor of nitric acid, has been carried out since 1906 through the Ostwald process involving NH_3 oxidation [1]. Pt-Rh catalytic gauzes are operated at high temperatures (840–950 °C) and high linear velocities to limit the secondary reactions between the formed NO_x and unreacted NH_3 leading to N_2.

The NH_3 needed for the Ostwald process is synthesized from N_2 via an equally challenging reaction. It is carried out at the industrial scale through the Haber–Bosch process, first operated in 1913 based on iron catalysts [2]. The operating conditions are harsh, involving pressures up to 300 bars and temperatures between 450 and 550 °C.

More direct routes to NO_x, such as high-temperature reactions of air in an electric arc (Birkeland–Eyde process [3]) and fuel combustion [4] were abandoned as they were deemed poorly efficient. Yet, recent techno-economic analyses have shown that the Birkeland–Eyde process (leading to about 2% of NO) could be competitive with respect to the combined Haber–Bosch and Ostwald processes [3].

Microwave- and plasma-assisted catalysis are receiving increasing attention as efficient and practical technologies [5–8]. Plasma-assisted NO_x synthesis from N_2–O_2 mixtures has been studied for a few decades, usually at low pressures. Plasmas generated by radiofrequencies [9,10] and microwaves [11] in glass vessels at pressures up to 80 mBar were reported. The central roles of vibrationally excited N_2 molecules $N_2(X)_v$ in both the gas phase (Equation (1)) and at the surface (Equation (2)) of the vessel walls were proposed as follows:

$$N_2(X)_v + O(^3P) \rightarrow NO + N \quad (1)$$

$$N_2(X)_{v-ads} + O_{ads} \rightarrow NO + N \quad (2)$$

Low pressures were needed to maximize the concentration of excited $N_2(X)_v$ states [11]. A two-fold increase in nitrogen fixation was observed when coating the vessel surface with catalysts, such as WO_3 and MoO_3, operating at a pressure of 40 mBar [10]. The rate-determining step proposed was the reaction between vibrationally excited N_2 molecules and surface oxygen (Equation (2)).

Other examples have been reported on the production of NO_x directly from air at low temperatures. Non-thermal plasma (NTP) catalytic double barrier discharge (DBD) reactors, typically operated at atmospheric pressure, showed promising results [12]. Using a MnO_x/γ-Al_2O_3 catalyst allowed forming up to 800 ppm of NO_x [13]. Patil et al. reported work on several oxides, and up to 5700 ppm of NO_x (=NO + NO_2) was formed at a residence time of 0.4 s over γ-alumina [14]. A WO_3/γ-Al_2O_3 catalyst increased the NO_x concentration further by about 10% compared to γ-Al_2O_3, while oxidation catalysts such as Co_3O_4, PbO, V_2O_5, NiO, MoO_3, and CuO only provided minor or no improvement. More recent work reported NO_x concentrations up to 1% using a similar NTP catalytic DBD either empty or filled with γ-alumina needles [15].

Microkinetic modeling concerning the combination of radiofrequency-generated NTP with Pt-based catalysts to produce NO from air placed the emphasis on the reactions taking place on the Pt surface between NTP-derived radicals and vibrationally excited molecules [16]. Note that the total pressure used was only 5 mBar.

Processes for nitrogen fixation (to NO_x and NH_3) using plasma reactors were recently proposed [17]. Recent patents [18–20] also reported the utilization of microwave-excited hot plasma (MWP) reactors for the oxidation of N_2, which are promising technologies for decarbonized and energy-efficient processes [21]. The quenching of NO in hot plasmas has yet been noted as a crucial point necessary to limit NO decomposing back to N_2 and O_2 [11].

We recently investigated CO_2 trapping–methanation [22,23] and pollutant catalytic combustion [24] assisted by microwaves (MWs) using quartz reactors located in domestic MW ovens. MWs allow selectively heating catalysts/sorbents and not the quartz reactor and gaseous stream, thereby offering obvious energy-saving opportunities. The fact that only the susceptor/catalyst heats up also limits undesirable gas-phase reactions such as product (e.g., NO) decomposition [25]. In addition, heating rates can be as high as a few 100 s °C s^{-1}, as observed in the case of a La-Ce-Mn-O perovskite that glows red in less than 3 s after turning on the MW power [24,26]. Brief occurrences of hot plasma triggered by MWs were noticeable when using this La-Ce-Mn-O perovskite [26].

NO_x formation has been reported upon the MW-irradiation of SiO_2-supported $BaTiO_3$ perovskites in air, although NO_x concentrations higher than 500 ppm could not be measured [27]. The formation of NO_x from air over perovskites is not surprising, as La- and Mn-based perovskites are well-known catalysts for NO_x decomposition into N_2 and O_2, which is the reverse reaction to that of interest here [28–32]. The formation of NO_x from N_2–O_2 mixtures while MW irradiating an unsupported La-Ce-Mn-O perovskite located in a quartz flow reactor is reported here. The reactor was studied at atmospheric pressure, representing more practical operating conditions than the low pressures often used before. NO_x concentration in excess of 2 vol.% could be obtained through a hot plasma triggered by the microwaves, which is a significant achievement in comparison to previous reports. Reaction mechanisms and energy balance should also be determined, but are outside the scope of the present report.

2. Results and Discussion

Figure 2A shows a picture of the La-Ce-Mn-O material after 2 min under a nominal MW power of 300 W. The measure of temperature in MW cavities is typically difficult [25,33,34]

and was grossly estimated here based on the sample glowing color (black body radiation [35]). An orange color indicated temperatures higher than 700 °C, though the emission was not uniform throughout the bed. This observation pointed to zones of much lower temperatures, likely due to the heterogeneity of the electric field around the bed (Figure S2).

No NO_x formation was observed over the whole duration of the experiment (Figure 2B). Traces of CO_2 were noted due to the decomposition of carbonate species present on the sample, as evidenced by DRIFTS spectroscopy of the fresh material (Figure S3A).

The power was increased to 600 W in the subsequent run. A strong brilliance in the white color associated with plasma was observed after only about 10 s (Figure 1A). NO_2 was the main reaction product with a concentration as high as 16,500 ppm (Figures 1B and S4). The concentration of NO reached ca. 8500 ppm, while N_2O was not observed. N_2O_4, the dimer of NO_2, was also formed at a concentration of 475 ppm, less than 2% of the total NO_x observed here, and this molecule will be neglected thereafter. NO_2 and its dimer were probably formed in the setup dead volume after the catalyst bed by the facile homogeneous low-temperature reaction between NO and O_2 [36], as this reaction is thermodynamically not favored at high temperatures [37].

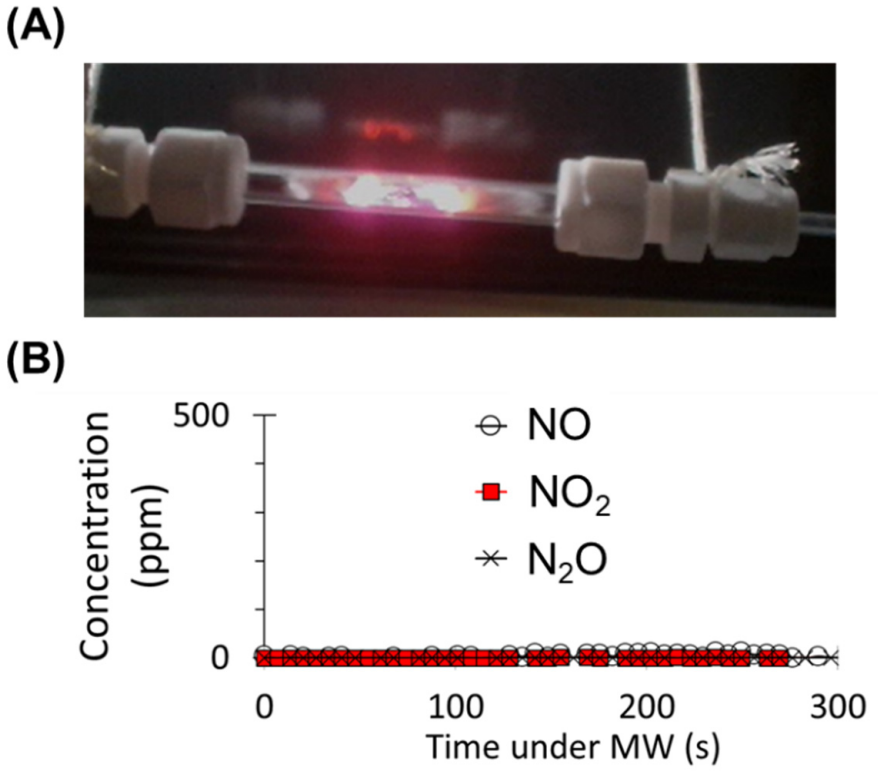

Figure 1. (**A**) Picture of the glowing La-Ce-Mn-O material after ca. 10 s under MW irradiation at a nominal power of 600 W. Video S1 and reference [38]. (**B**) Corresponding concentration of NO_x formed as a function of time. Feed composition: 20% O_2 + 80% N_2, Total flow rate = 50 mL min^{-1}. Sample mass = 130 mg.

The MW irradiation was stopped after only 27 s in this case to prevent any potential damage to the PTFE fittings and quartz reactor. Part of the quartz wool located near the plasma had melted during the experiment, stressing that very high temperatures were reached, as the melting point of quartz is around 1700 °C. A video of the La-Ce-Mn-O material under 300 and 600 W is given in Video S1 and is also available online [38].

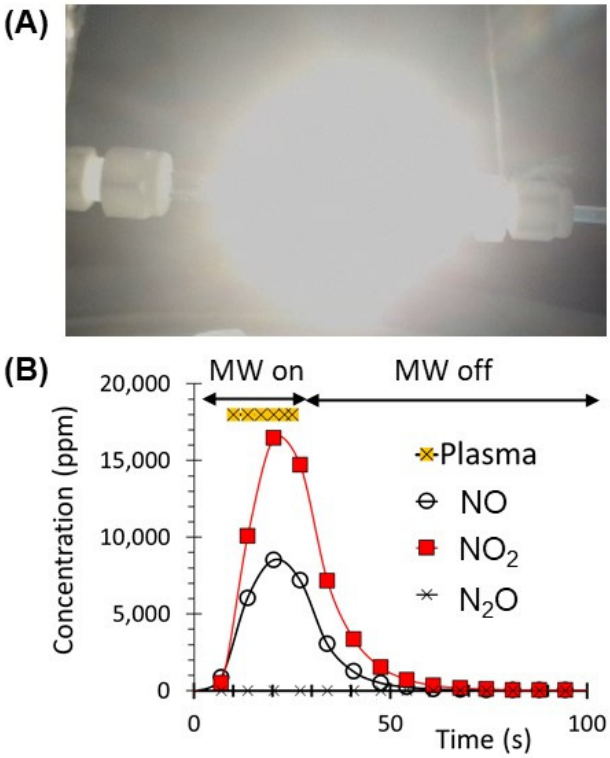

Figure 2. (**A**) Picture of the glowing La-Ce-Mn-O material after 2 min under MW irradiation at a nominal power of 300 W. Video S1 and link in reference [38]. (**B**) Corresponding concentrations of NO_x, showing that no N_2 fixation took place under these conditions. Feed composition: 20% O_2 + 80% N_2, Total flow rate = 50 mL min^{-1}. Sample mass = 130 mg.

The highest NO_x concentration observed during the 600 W experiment (Figure 1B) was ca. 25,500 ppm = 2.5%. A plot of the thermodynamic equilibrium between O_2, N_2, NO, and NO_2 is given in Figure 3. A concentration of 25,500 ppm under the present 20% O_2 + 80% N_2 feed would be reached thermally at around 2300 °C. Whether this was the actual temperature within the hottest spots of the reactor or a microwave effect taking place enabled the reaction to proceed at much lower temperatures is unclear [25,39,40].

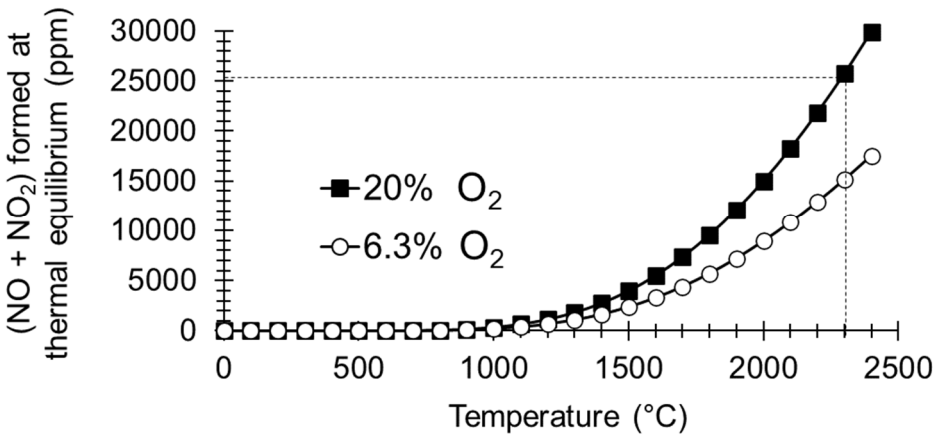

Figure 3. Thermodynamic equilibrium between O_2, N_2, NO, and NO_2 as a function of temperature for 20 and 6.3 vol.% of dioxygen in the initial O_2 + N_2 mixture. The pressure was set at 1 bar. Calculated using HSC Chemistry 6.2 software.

It is also difficult to determine whether the reaction was solely heterogeneous or partly/wholly homogeneous. The strong temperature gradients present in the La-Ce-Mn-O catalyst

bed complicate any quantitative analysis of the experiment. The density of hot spots and the temperature of those were not controlled and not easily measurable. Therefore, it is difficult to relate the catalyst weight, the bed dead volume, and the observed reaction rate. In addition, it is likely that bed packing also affected plasma generation, complicating the analysis of the relationship between reaction rates and bed voids necessary to demonstrate the occurrence of gas-phase reactions. More work is needed to clarify this very important aspect.

Reactions were subsequently carried out at lower O_2 partial pressures to limit NO_2 and N_2O_4 formation. Lower MW power inputs were also used to reduce thermal stress on the equipment. Interestingly, plasma and NO_x could be obtained at only 100 W of nominal power (Figure 4) once the material has been irradiated at a higher power (typically 600 W), leading to plasma formation. We believe that this activation was related to the sintering of the La-Ce-Mn-O powder that led to particle sizes that were more suitable for MW absorption (*vide infra*). NO was the main reaction product under these conditions, and the level of N_2O_4 was negligible (see black spectrum in Figure 5).

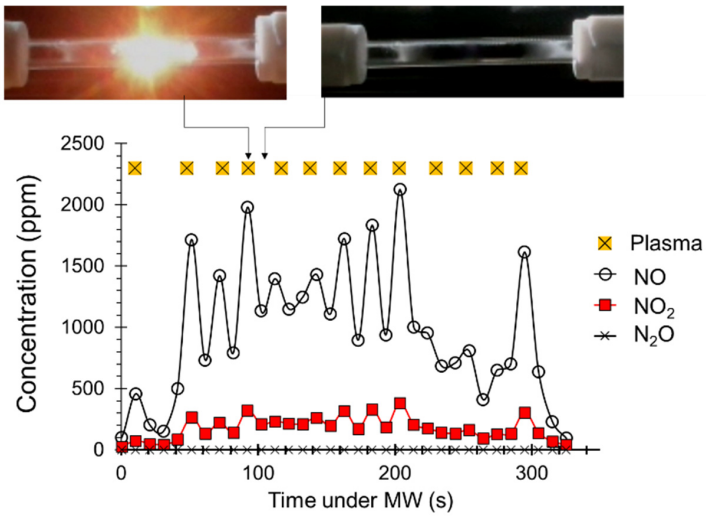

Figure 4. Evolution of NO_x concentrations over time under a nominal power of 100 W. The pictures show the sample emission at two different times corresponding to high and low NO_x production. Feed composition: 6.3% O_2 + 93.7% N_2, Total flow rate = 40 mL min^{-1}. Sample mass = 200 mg. The sample has been treated earlier at 600 W for activation.

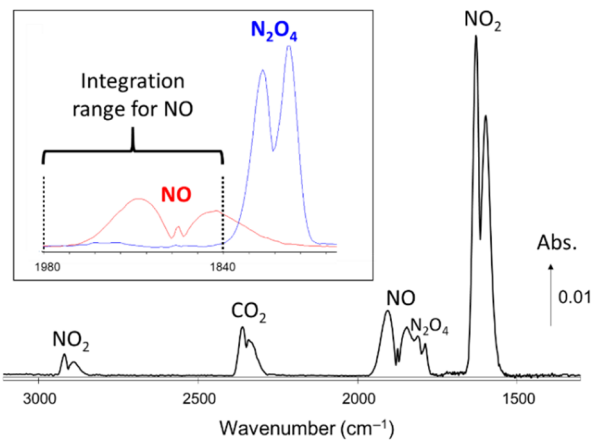

Figure 5. Typical FT-IR transmission IR spectrum showing the various reaction products (black spectrum), which was obtained at MW power = 100 W after activation at 600 W under flowing 6.3% O_2 in N_2. The inset shows the overlapping of NO (red spectrum) and N_2O_4 (blue spectrum) IR bands and the integration range used for NO.

The NO and NO_2 signals and the plasma occurrence were not steady at this power setting of 100 W. A video of the experiment [41] shows that the material glowed periodically, stressing that the power delivery was pulsed. This is typical of a domestic MW oven, despite the manufacturer's claim that the present Inverter MW oven should have been delivering power in a continuous mode. The pulsed nature of power delivery at 100 W of this specific MW oven was confirmed in our recent study on CO_2 methanation [23]. The fact that heating, and thereby the reaction, periodically shut down was thus merely related to the off-period of the MW magnetron. This pulse procedure may have actually prevented damages to the quartz reactor and perovskite susceptor by enabling excess heat to diffuse away during the off-period.

The maxima of NO_x (mostly NO) formation were clearly correlated to the appearance of the plasmas (Figure 4). A careful perusal of the video [41] of the experiment revealed the presence of micro-plasma events that did not always spread out and which were located in specific locations of the catalytic bed.

It should also be stressed that the bed was not tightly compressed in between the quartz wool plugs and that the catalyst powder could move within this space. The video (Video S1 and reference [38]) of the experiment reported in Figure 1 at 600 W shows that the sample powder moved during the plasma episode. Such loose packing of the catalyst powder led irremediably to difficulty in controlling the heating of the material and required sample repositioning within the quartz reactor. The loose packing was yet necessary to induce plasma formation through the presence of empty volumes that limit charged particle recombination. More work will be required to disentangle these crucial aspects.

A DRIFTS analysis of the sample after the production of NO and NO_2 (Figure S3B) did not reveal the presence of adsorbed NO_x species, stressing that most products formed left the reactor. An XRD analysis indicated minor structural changes after repeated uses and plasma generation, while the main crystalline phases present were still $LaMnO_{3.15}$ and CeO_2 (Figure S5). The proportion of minor perovskite phases of $LaMnO_3$ (PDF 01-076-9087) and $La_2Ce_2O_{6.72}$ decreased, while that of $LaMnO_{3.00}$ (PDF 00-035-1353) increased. This suggests a partial segregation of Ce and La. No evidence of spinel phase formation following plasma occurrence was evidenced, in contrast to an earlier report [27].

The presence of agglomerated sample powder and molten quartz wool were noted after plasma generation. The melting point of La-based perovskites ranged from 1900 up to 2100 °C [42]. The high temperatures reached around the plasma zones and thus led to some sintering of the La-Ce-Mn-O particles. The BET of the aged sample could not be measured reliably, but was close to zero within the experimental error (the original sample presented a mere BET surface area of 4 m^2 g^{-1}).

More work is needed to fully comprehend the parameters controlling the formation of NO_x and the role of plasma during the microwave irradiation over the La-Ce-Mn-O material. The sample composition, bed packing, particle size, duration, and frequency of the plasma events (including activation by aging) may all be crucial.

The point of contact between particles was actually shown to exacerbate hot spots in the case of SiC [43] and grapes [44], even leading to plasma generation in the latter case. Further work is required to understand this perovskite-based system that offers great promise for efficient nitrogen fixation using inexpensive reactor materials and microwave sources. Operating conditions and energy balance will also have to be considered.

3. Experimental Section

The La-Ce-Mn-O (nominal composition $La_{0.8}Ce_{0.2}MnO_3$) sample was prepared according to a method reported earlier ([45] and Supplementary Materials) and used without further pre-treatment. The large La and Ce cations occupy the A-type sites of the perovskite structure, while Mn cations occupy B sites [46,47]. The experimental setup is described in Figure 6. N_2 and O_2 (high purity gasses from Air Liquid, Paris, France) were fed through Brooks electronic mass flow controllers (Brooks Instrument, Hatfield, PA, USA). The catalytic experiments were carried out at atmospheric pressure and at a total flowrate of 50 or

40 mL min^{-1}. The gasses could be sent first to the quartz reactor placed inside a Panasonic microwave oven (1000 W, Inverter model NN-SD28HSGTG, operating at 2.45 GHz, Panasonic, Kadoma, Japan) or directly to the IR analyzer. The IR analyzer comprised a Harrick 10 cm-pathlength gas cell (dead-volume of 17 mL, Harrick, Pleasantville, NY, USA), kept at 80 °C and placed in a Bruker Tensor 27 spectrophotometer (Bruker, Ettlingen, Germany). The gas cell was used to measure NO, N_2O, and NO_2 IR signals in the reactor effluent (Figure 5). The IR spectra were recorded at a resolution of 4 cm^{-1}, and four scans were averaged and analyzed with the OPUS 6.0 software.

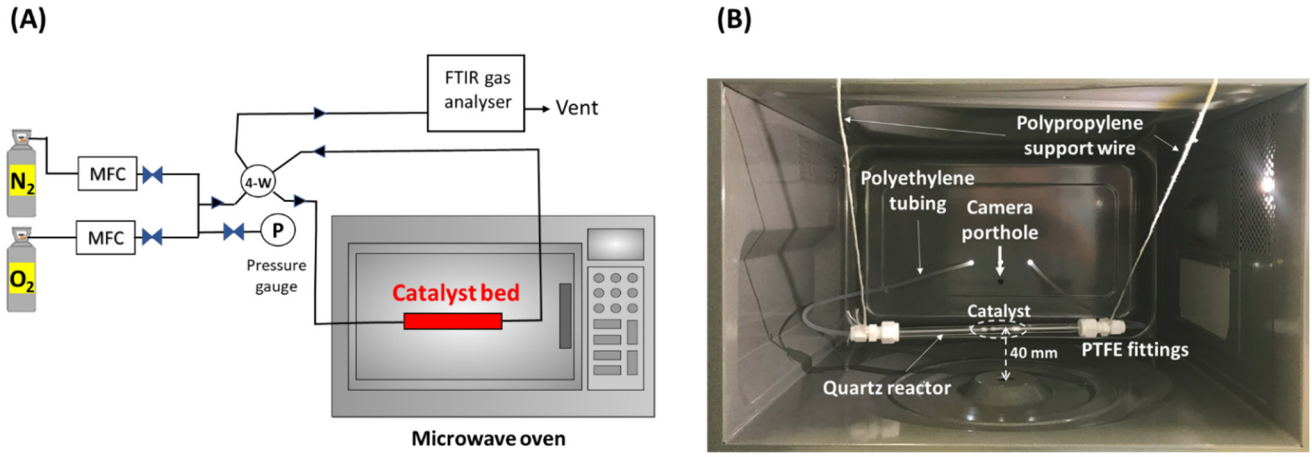

Figure 6. (**A**) Schematic representation of the experimental setup. (**B**) Picture of the microwave cavity showing the quartz reactor, PTFE fittings, and polyethylene tubings. The catalyst powder was held by quartz wool plugs. The catalyst bed was located at 40 ± 5 mm from the oven bottom center.

The concentrations of NO, NO_2, and N_2O (never detected here) were determined through the IR band areas and references spectra. The N_2O and NO_2 signals were integrated over 2250–2175 cm^{-1} and 1700–1500 cm^{-1}, respectively (see Figure S1 for details). The NO signal was integrated over 1980–1840 cm^{-1} to avoid overlapping with N_2O_4.

The concentration of N_2O_4, the dimer of NO_2, was estimated based on the intensity of its band near 1800 cm^{-1}, since it corresponds to the asymmetric stretching vibration of the O-N-O group, which is observed at 1600 cm^{-1} in the case of the monomer NO_2. It was assumed that the molar extinction coefficient of these two modes were equal. The area of this 1800 cm^{-1} N_2O_4 band in most experiments was significantly smaller than that of the 1600 cm^{-1} band of NO_2, and its contribution to the NO_x formed was essentially negligible.

The location of the electromagnetic standing waves is uneven in multimodal MW ovens [48], hence the main heating zones were determined using thermal paper (Figure S2). The heating position near the cavity center was selected as the location of the catalyst bed.

Powder X–ray diffraction patterns (XRDs) were recorded to assess the crystalline phases present. Diffractograms were collected between 10 and 80° (2Θ) with steps of 0.02° and 1 s per step with a Bruker D8-Advance diffractometer using CuKα radiation at λ = 1.5418 Å (Bruker, Ettlingen, Germany). BET surface areas were measured at 77 K on an ASAP 2020 from Micromeritics (Norcross, GA, USA). Samples were first outgassed under vacuum at 300 °C for 3 h. Ex situ diffuse reflectance FT-IR (DRIFTS) analysis was conducted in a setup described elsewhere [22].

4. Conclusions

Significant concentrations of NO and NO_2 could be obtained by flowing N_2 + O_2 mixtures over a La-Ce-Mn-O perovskite material located in a quartz flow reactor irradiated by microwaves. NO_x generation correlated with the generation of hot plasmas. The effective reaction temperature and the proportion of heterogeneous and homogeneous reactions taking place are yet unclear. This system offers great promise as an efficient

nitrogen fixation process through reactor electrification due to the fast response offered by the La-Ce-Mn-O in terms of temperature heating and shut down.

Supplementary Materials: The following supporting information can be downloaded at: https://www.mdpi.com/article/10.3390/catal14090635/s1, Figure S1: Detailed integration parameters for NO, N_2O, and NO_2, Figure S2: Picture of cardboard-supported thermal paper used to determine the location of heating zones in the microwave cavity; Figure S3: Diffuse reflectance FT-IR spectra of the fresh and used La-Ce-Mn-O material, Figure S4: FT-IR transmission IR spectrum corresponding to the maximum of NO_x formation during the plasma pulse observed under 600 W MW power, Figure S5: X-ray diffraction patterns of the fresh and used La-Ce-Mn-O material. Video S1: Video of the La-Ce-Mn-O material exposed to 300 (top) and 600 (bottom) W of MW power under a flow of 20% O_2 + 80% N_2. Ref. [49] is cited in the Supplementary Materials.

Author Contributions: F.C.M. conceptualized the work. F.C.M. and A.K. carried out the experiments. F.C.M. prepared the draft of the paper and all authors contributed to the final version. All authors have read and agreed to the published version of the manuscript.

Funding: This research received no external funding.

Data Availability Statement: The raw data supporting the conclusions of this article will be made available by the authors on request.

Conflicts of Interest: The authors declare no competing financial interest.

References

1. Thiemann, M.; Scheibler, E.; Wiegand, K.W. Nitric Acid, Nitrous Acid, and Nitrogen Oxides. In *Ullmann's Encyclopedia of Industrial Chemistry*; Elvers, B., Ed.; Verlag Chemie: Hoboken, NJ, USA, 2000. [CrossRef]
2. Appl, M. Ammonia. In *Ullmann's Encyclopedia of Industrial Chemistry*; Elvers, B., Ed.; Verlag Chemie: Hoboken, NJ, USA, 2006. [CrossRef]
3. Rouwenhorst, K.H.R.; Jardali, F.; Bogaerts, A.; Lefferts, L. Correction: From the Birkeland–Eyde process towards energy-efficient plasma-based NO_X synthesis: A techno-economic analysis. *Energy Environ. Sci.* **2021**, *16*, 6170–6173. [CrossRef]
4. Thompson, D.; Brown, T.D.; Beer, J.M. NO_x formation in combustion. *Combust. Flame* **1972**, *19*, 69–79. [CrossRef]
5. Pimenta, F.; Filho, E.; Diniz, Â.; Barrozo, M.A.S. Catalytic Microwave-Assisted Pyrolysis of the Main Residue of the Brewing Industry. *Catalysts* **2023**, *13*, 1170. [CrossRef]
6. Sakurada, N.; Kitazono, T.; Ikawa, T.; Yamada, T.; Sajiki, H. Pt/CB-Catalyzed Chemoselective Hydrogenation Using In Situ-Generated Hydrogen by Microwave-Mediated Dehydrogenation of Methylcyclohexane under Continuous-Flow Conditions. *Catalysts* **2024**, *14*, 384. [CrossRef]
7. Arshad, M.Y.; Ahmad, A.S.; Mularski, J.; Modzelewska, A.; Jackowski, M.; Pawlak-Kruczek, H.; Niedzwiecki, L. Pioneering the Future: A Trailblazing Review of the Fusion of Computational Fluid Dynamics and Machine Learning Revolutionizing Plasma Catalysis and Non-Thermal Plasma Reactor Design. *Catalysts* **2024**, *14*, 40. [CrossRef]
8. Cheng, H.; Ren, X.; Yao, Y.; Tang, X.; Yi, H.; Gao, F.; Zhou, Y.; Yu, Q. Application of Unconventional External-Field Treatments in Air Pollutants Removal over Zeolite-Based Adsorbents/Catalysts. *Catalysts* **2023**, *13*, 1461. [CrossRef]
9. Amouroux, J.; Cavvadias, S.; Rapakoulias, D. Réacteur de synthèse et de trempe dans un plasma hors d'équilibre: Application à la synthèse des oxydes d'azote. *Rev. Phys. Appl.* **1979**, *14*, 969–976. [CrossRef]
10. Rapakoulias, D.; Cavadias, S.; Amouroux, J. Processus catalytiques dans un réacteur à plasma hors d'équilibre II. Fixation de l'azote dans le système N2-O2. *Rev. Phys. Appl.* **1980**, *15*, 1261–1265. [CrossRef]
11. Mutel, B.; Dessaux, O.; Goudmand, P. Energy cost improvement of the nitrogen oxides synthesis in a low pressure plasma. *Rev. Phys. Appl.* **1984**, *19*, 461–464. [CrossRef]
12. Sun, G.; Zhu, A.; Yang, X.; Niua, J.; Xu, Y. Formation of NO_x from N_2 and O_2 in catalyst-pellet filled dielectric barrier discharges at atmospheric pressure. *Chem. Commun.* **2003**, *12*, 1418–1419. [CrossRef]
13. Zhang, T.-Q.; Li, X.-S.; Liu, J.-L.; Wen, X.-Q.; Zhu, A.-M. Plasma Nitrogen Fixation: NO_x Synthesis in MnO_x/Al_2O_3 Packed-Bed Dielectric Barrier Discharge. *Plasma Chem. Plasma Proc.* **2023**, *43*, 1907–1919. [CrossRef]
14. Patil, B.S.; Cherkasov, N.; Lang, J.; Ibhadon, A.O.; Hessel, V.; Wang, Q. Low temperature plasma-catalytic NO_x synthesis in a packed DBD reactor: Effect of support materials and supported active metal oxides. *Appl. Catal. B Environ.* **2016**, *194*, 123–133. [CrossRef]
15. Li, Y.; Qin, L.; Wang, H.-L.; Li, S.-S.; Yuan, H.; Yang, D.-Z. High efficiency NO_x synthesis and regulation using dielectric barrier discharge in the needle array packed bed reactor. *Chem. Eng. J.* **2023**, *461*, 141922. [CrossRef]
16. Ma, H.; Sharma, R.K.; Welzel, S.; van de Sanden, M.C.M.; Tsampas, M.N.; Schneider, W.F. Observation and rationalization of nitrogen oxidation enabled only by coupled plasma and catalyst. *Nat. Commun.* **2022**, *13*, 402. [CrossRef] [PubMed]

17. Hollevoet, L.; Vervloessem, E.; Gorbanev, Y.; Nikiforov, A.; De Geyter, N.; Bogaerts, A.; Martens, J.A. Energy-Efficient Small-Scale Ammonia Synthesis Process with Plasma-Enabled Nitrogen Oxidation and Catalytic Reduction of Adsorbed NO_x. *ChemSusChem* **2022**, *15*, e202102526. [CrossRef] [PubMed]
18. Bell, R.S.E.; Cupertino, D. Production of Nitrogen Oxides. World Patent WO2020115473A1, 3 December 2019.
19. Forsberg, G.; Baeling, P.; Van Rooij, G.J. Method for the Synthesis of Nitrogen Oxides and Nitric Acid in a Thermal Reactor. World Patent WO2022159018A1, 18 January 2022.
20. McEnamey, J.; Schwalbe, J.A.; Chocklingam, S.; Pinkowski, N. Microwave Plasma System for Efficiently Producing Nitric Acid and Nitrogen Fertilizers. World Patent WO2023137047A1, 11 January 2023.
21. Radoiu, M.; Mello, A. Scaling up microwave excited plasmas—An alternative technology for industrial decarbonization. *Plasma Processes Polym.* **2024**, *21*, e2300200. [CrossRef]
22. Acher, L.; Laredo, T.; Caillot, T.; Kaddouri, A.; Meunier, F.C. Trapping and Methanation of CO_2 in a Domestic Microwave Oven Using Combinations of Sorbents and Catalysts. *Appl. Sci.* **2023**, *13*, 12536. [CrossRef]
23. Acher, L.; Gana, J.; Caillot, T.; Kaddouri, A.; Meunier, F.C. CO_2 capture and methanation over iron and cobalt-containing catalysts operated in a domestic microwave oven. *Appl. Catal. A Gen.* **2024**, *685*, 119898. [CrossRef]
24. Perroud, H.; Miraux, J.; Lions, M.; Caillot, T.; Ferronato, C.; Kaddouri, A.; Meunier, F.C. Combustion of volatile organic compounds in a domestic microwave oven using regenerable sorbent-catalyst combinations. *Sep. Purif. Technol.* **2024**, *330*, 125387. [CrossRef]
25. Palma, V.; Barba, D.; Cortese, M.; Martino, M.; Renda, S.; Meloni, E. Microwaves and Heterogeneous Catalysis: A Review on Selected Catalytic Processes. *Catalysts* **2020**, *10*, 246. [CrossRef]
26. Link to a Video Showing the Fast Heating of a La-Ce-Mn-O Perovskite in Comparision to a CuO-Based Sample. Available online: https://sdrive.cnrs.fr/s/xY63sGTLxNRENH9 (accessed on 18 September 2024).
27. Akay, G. Plasma Generating—Chemical Looping Catalyst Synthesis by Microwave Plasma Shock for Nitrogen Fixation from Air and Hydrogen Production from Water for Agriculture and Energy Technologies in Global Warming Prevention. *Catalysts* **2020**, *10*, 152. [CrossRef]
28. Teraoka, Y.; Fukuda, H.; Kagawa, S. Catalytic Activity of Perovskite-Type Oxides for the Direct Decomposition of Nitrogen Monoxide. *Chem. Lett.* **1990**, *19*, 1–4. [CrossRef]
29. Teraoka, Y.; Harada, T.; Kagawa, S. Reaction mechanism of direct decomposition of nitric oxide over Co- and Mn-based perovskite-type oxides. *J. Chem. Soc. Faraday Trans.* **1998**, *94*, 1887–1891. [CrossRef]
30. Ishihara, T.; Ando, A.; Takiishi, K.; Yamada, K.; Nishiguchi, H.; Takita, Y. Direct decomposition of NO into N_2 and O_2 over La(Ba)Mn(In)O_3 perovskite oxide. *J. Catal.* **2003**, *220*, 104–114. [CrossRef]
31. Onrubia-Calvo, J.A.; Pereda-Ayo, B.; González-Velasco, J.R. Perovskite-Based Catalysts as Efficient, Durable, and Economical NO_x Storage and Reduction Systems. *Catalysts* **2020**, *10*, 208. [CrossRef]
32. Zhao, D.; Song, H.; Liu, J.; Jiang, Q.; Li, X. Advances in Designing Efficient La-Based Perovskites for the NO_x Storage and Reduction Process. *Catalysts* **2022**, *12*, 593. [CrossRef]
33. Kalinke, I.; Kubbutat, P.; Dinani, S.T.; Ambros, S.; Ozcelik, M.; Kulozik, U. Critical assessment of methods for measurement of temperature profiles and heat load history in microwave heating processes—A review. *Comp. Rev. Food Sci. Food Saf.* **2022**, *21*, 2118–2148. [CrossRef] [PubMed]
34. Bao, C.; Serrano-Lotina, A.; Niu, M.; Portela, R.; Li, Y.; Lim, K.H.; Liu, P.; Wang, W.-J.; Banares, M.A.; Wang, Q. Microwave-associated chemistry in environmental catalysis for air pollution remediation: A review. *Chem. Eng. J.* **2023**, *466*, 142902. [CrossRef]
35. Available online: https://en.wikipedia.org/wiki/Black-body_radiation (accessed on 5 September 2024).
36. Mochida, I.; Kawabuchi, Y.; Kawano, S.; Matsumura, Y.; Yoshikawa, M. High catalytic activity of pitch-based activated carbon fibres of moderate surface area for oxidation of NO to NO_2 at room temperature. *Fuel* **1997**, *76*, 543–548. [CrossRef]
37. Meunier, F.C.; Breen, J.P.; Ross, J.R.H. New insights into the origin of NO_2 in the mechanism of the selective catalytic reduction of NO by propene over alumina. *Chem. Commun.* **1999**, *3*, 259–260. [CrossRef]
38. Link to a Video Showing the Emission of the La-Ce-Mn-O at 300 and 600 W. Available online: https://sdrive.cnrs.fr/s/6SnNfgQnCPafX5X (accessed on 18 September 2024).
39. Hunt, J.; Ferrari, A.; Lita, A.; Crosswhite, M.; Ashley, B.; Stiegman, A.E. Microwave-Specific Enhancement of the Carbon–Carbon Dioxide (Boudouard) Reaction. *J. Phys. Chem. C* **2013**, *117*, 26871–26880. [CrossRef]
40. Wang, X.; Wang, Y.; Robinson, B.; Caiola, A.; Hu, J. Selectivity modulated oxidative dehydrogenation of ethane with CO_2 under microwave catalytic processing. *Catal. Sci. Technol.* **2023**, *13*, 34993504. [CrossRef]
41. Link to a Video Showing the Pulsation of the Emission of the La-Ce-Mn-O at 100 W. Available online: https://sdrive.cnrs.fr/s/aaDyi7wnbW97LXT (accessed on 18 September 2024).
42. Kuscer, D.; Hrovat, M.; Holc, J.; Bernik, S.; Kolar, D. Phases in the $LaMnO_{3\pm\delta}$–$SrMnO_{3-\delta}$–$LaAlO_3$ system. *Mater. Res. Bull.* **2000**, *35*, 2525–2544. [CrossRef]
43. Haneishi, N.; Tsubaki, S.; Abe, E.; Maitani, M.M.; Suzuki, E.I.; Fujii, S.; Fukushima, J.; Takizawa, H.; Wada, Y. Enhancement of Fixed-bed Flow Reactions under Microwave Irradiation by Local Heating at the Vicinal Contact Points of Catalyst Particles. *Sci. Rep.* **2019**, *9*, 222. [CrossRef]
44. Khattak, H.K.; Bianucci, P.; Slepkov, A.D. Linking plasma formation in grapes to microwave resonances of aqueous dimers. *Proc. Natl. Acad. Sci. USA* **2019**, *116*, 4000–4005. [CrossRef]

45. Kaddouri, A.; Ifrah, S. Microwave-assisted synthesis of $La_{1-x}B_xMnO_{3.15}$ (B = Sr, Ag; x = 0 or 0.2) via manganese oxides susceptors and their activity in methane combustion. *Catal. Commun.* **2006**, *7*, 109–113. [CrossRef]
46. Bhalla, A.S.; Guo, R.; Roy, R. The perovskite structure—A review of its role in ceramic science and technology. *Mater. Res. Innov.* **2000**, *4*, 3–26. [CrossRef]
47. Keav, S.; Matam, S.K.; Ferri, D.; Weidenkaff, A. Structured Perovskite-Based Catalysts and Their Application as Three-Way Catalytic Converters—A Review. *Catalysts* **2014**, *4*, 226–255. [CrossRef]
48. Monteiro, J.; Costa, L.C.; Valente, M.A.; Santos, T.; Sousa, J. Simulating the electromagnetic field in microwave ovens. In Proceedings of the 2011 SBMO/IEEE MTT-S International Microwave and Optoelectronics Conference (IMOC 2011), Natal, Brazil, 29 October–1 November 2011; pp. 493–497. Available online: https://ieeexplore.ieee.org/document/6169274 (accessed on 18 September 2024).
49. Muhumuza, E.; Wu, P.; Nan, T.; Zhao, L.; Bai, P.; Mintova, S.; Yan, Z. Perovskite-Type $LaCoO_3$ as an Efficient and Green Catalyst for Sustainable Partial Oxidation of Cyclohexane. *Ind. Eng. Chem. Res.* **2020**, *59*, 21322–21332. [CrossRef]